STUDY ON THE SUBSTRUCTURAL EVOLUTION OF AA3104 ROLLED SHEET DURING THERMAL TREATMENTS

Sofia M. Papadopoulou[1,2]*, Athanasios Vazdirvanidis[1], Spyros Papaefthymiou[2]

[1]Hellenic Research Centre for Metals (ELKEME), 61st km Athens-Lamia National Road, Oinofyta 32011, Greece

[2]National Technical University of Athens (NTUA),9 Heroon Polytechniou Str., Zografou 15780, Greece

Abstract

The substructure of the rolled sheets plays a significant role as well as grain structure in the control of mechanical properties. The features that consist the substructure are prone to significant alterations throughout the production process and they require high-magnification and high-resolution analysis. . The present paper focuses on the study of the substructural evolution of a cold-rolled AAA3104 sheet during recovery and recrystallization thermal treatments. The results are correlated to the respective r-values and subgrain boundaries properties. The optimal behavior regarding formability was observed in the partially recrystallized sample (H28) accompanied by the presence of ≈14% subgrain angle boundaries (2-5° misorientation) and comparable recrystallization and deformation texture components.

Keywords: *substructure, AA3104, EBSD, thermal treatment, recovery, recrystallization*

1. INTRODUCTION

The Al products exhibit many desired properties and therefore are used for several applications [1], [2]. Some of them are in food industry, in automotive, in aerospace etc. [3]-[5]. Even though the Al alloys, their production process and their microstructural aspects have been studied for decades [6]-[9], many challenging aspects are not studied thoroughly [10], [11]. Such aspects are the evolution of the substructure during common industrial stages and its correlation to the formability of the Al sheet. Formability is correlated to anisotropy of the Al sheets since during deep drawing is observed the so-called earing phenomenon [12]-[15]. Studies have shown that there is correlation between the location of the ears on the formed cup and the texture components of the sheet [13], [14], [16]-[18]. Regarding the Al sheet texture, the three main categories under investigation are rolling, recrystallization and random texture [11], [15], [19]-[22]. The rolling texture in Al is mainly composed of the S, Brass and Copper orientations. The β fiber is generally prominent in rolling textures. In orientation space the fiber runs from the copper to the brass component. The S orientations are at intermediate locations of this fiber [19]. Rolling texture components promote earing essentially at 45°/135° with respect to the rolling direction. Concerning earing, low ear ratio can be composed by a suitable combination of crystals with an orientation that results in 45°/135° ears and those that produce 0°/90° ears [2], [3]. Recrystallization textures depend on stacking fault energy (SFE), the prior deformed state, the annealing temperature and particularly the precipitation state. The balance between deformation textures and annealing textures is crucial to controlling earing in beverage can stock [1]. In the present work, the evolution of the substructure of a cold-rolled AA3104 sheet during recovery and recrystallization thermal treatments is observed in order to understand deeper each state and the effect of the substructure towards formability.

2. MATERIALS AND METHODS

The AA 3104 alloy sheet samples (Table 1) that were examined were produced through direct chill (DC) casting and originated from a 600 mm thickness plate. After hot and cold rolling thermal treatments of final gauge sample were performed for achievingH19, H24, H28 and O metallurgical conditions. Samples' designation was selected according to BS EN 541:2006 [23].

Table 1. Chemical composition of the examined samples according to [24].

Elements (%)									
Al	**Mn**	**Mg**	**Fe**	**Si**	**Cu**	**Ti**	**Ga**	**V**	**Zn**
95.0-98.4	0.80-1.4	0.80-1.3	≤0.80	≤0.60	0.05-0.25	≤0.10	≤0.05	≤0.05	≤0.25

2.1. Tensile Testing

Specimens from all metallurgical conditions were subjected to uniaxial tensile testing, as per the requirements of the ISO 6892-1 testing standard. In particular, the Rp (yield strength—YS), Rm (ultimate tensile strength—UTS) and Ag (elongation) parameters were measured. The tensile specimens were cut, in orientations of 0°, 45° and 90° relevant to the RD.

Anisotropy of the sheets was evaluated by calculation of the ratio of plastic strain transverse to loading direction to plastic strain through thickness during the tensile tests [19], [20]. This ratio is called the Lankford coefficient (r) and is a measure of plastic anisotropy of rolled sheets. R values are dependent on direction relative to rolling and constitute a critical indicator for formability of recrystallized low-carbon steel sheets as well as for Al flat-rolled products [21]. The Lankford coefficient is calculated during the tensile test, either by using elongation meters or by digital image correlation (DIC) [7], based on the following equation [25]:

$$r = \frac{\epsilon_w}{\epsilon_t} = \left\{ \frac{\ln \frac{w}{w_0}}{\ln \frac{t}{t_0}} \right\} \quad (1.1)$$

, where ε_w is the true width deformation, ε_t is the true thickness deformation, w_0 is the initial width of the tensile test, t_0 is the initial thickness of the tensile test, w is the final width of the tensile test and t is the final width of the tensile test. High values of the coefficient r indicate high resistance to thinning of the thickness direction [25].

However, the calculation of Lankford parameters for each of the directions (r_0, r_{45}, r_{90}) does not lead to a clear conclusion regarding the behavior of the plate during forming. For this reason, the parameter rm or is used, which is called "vertical anisotropy" ($\bar{r}$, normal anisotropy) and is a function of all three Lankford parameters as calculated from the relation [25]:

$$r_m = \bar{r} = \frac{(r_0 + r_{90} + 2r_{45})}{4} \quad (1.2)$$

The vertical anisotropy parameter describes the ability of the plate to shape in the direction of its thickness, relative to its surface, and is a parameter that is directly related to the limiting drawing ratio (LDR) parameter. For parameter values greater than one unit, the plate resists thinning, which is destructive to processes such as deep drawing, while the larger the unit's parameter, the better the material's behavior during deep drawing (higher drawability). For values $\bar{r}$ smaller than the unit, the risk of failure of the sheet during its deep drawing increases [25]. Another parameter used to evaluate the anisotropy of sheets, such as AA3104, is that of planar anisotropy (Δr), which is calculated as a function of the Lankford parameters from the relation [26]:

$$\Delta r = \frac{(r_0 + r_{90} - 2r_{45})}{2} \quad (1.3)$$

The planar anisotropy parameter is an indicator of the ability of the rolled material not to show differential plastic deformation during the deep drawing on the perimeter of the produced cup, i.e. not to present the undesired phenomenon of "earing".

2.2. Hardness and Conductivity Measurements

The Vickers method was used for hardness testing. A load of 0.2 kgf was selected for hardness measurements whereas for the electrical conductivity measurements, a frequency of 240 kHz was used. The mean values presented originate from the average of 10 measurements.

2.3. Optical Microscopy

The samples were cross-sectioned parallel to rolling direction and the specimens were cold mounted for avoiding annealing effects. Preparation was conducted by grinding and polishing, while grain structure was examined after Barker's electrolytic etch according to references [22] and [23], at 200× magnification. . Examination of the grain structure was performed with polarized light and by use of a Nikon Epiphot 300 inverted metallographic microscope (Nikon, Minato City, Tokyo, Japan).

2.4. Metallographic Examination—Texture

Microscopic analysis was performed using a JEOL IT-800 HL Scanning Electron Microscope (SEM, JEOL Ltd., Akishima, Tokyo, Japan) under a 20 kV accelerating voltage, coupled with an EDAX Apollo XF, equivalent to octane super EDS, silicon drift detector (SDD, EDAX, Mahwah, NJ, USA) in conjunction with TEAM (EDAX, Mahwah, NJ, USA) and SMILE VIEW™ Map software (JEOL Ltd., Akishima, Tokyo, Japancity, and Digital Surf, Besançon, France). EBSD analysis was carried out using an EDAX Hikari XP EBSD, high-speed camera (EDAX camera, EDEN Instruments SAS, Valence Cedex, France). When a polycrystalline metallic material, is subjected to thermomechanical processing, a dominant orientation, namely texture is observed. The texture could be formed through the deformation, annealing, or as a result of both processes. Texture can be categorized into several components, represented by {hkl}<uvw>. The latter are further divided into two groups, consisting of deformation and annealing texture components.

Calculation of the various texture components, resulting from the applied manufacturing process, was performed according to [19]:

-Rolling components: Copper {112}<111>, S2{213}<-1-42>, S3 (or S) {123}<634>, Taylor{4411}<11118>, Brass {011}<211>

-Recrystallization components: Cube {001}<100>, P{011}<111>, Q{013}<2-31>, R{124}<211>, Goss{011}<100>[24].

Electron backscatter diffraction (EBSD) analysis was performed on the longitudinal cross-section specimens (rolling direction coincided with TD and normal direction with ND coordinates) and the magnification used (100×–2000×) (examined areas 30 × 30 μm^2–150 × 150 μm^2). Calculation of the various texture components resulting from the applied manufacturing process (intermediate annealing and cold rolling) was performed.

EBSD scans were collected using hexagonal grid with 0.1-0.2 μm step. The SEM conditions for the scans were magnification of 200x, accelerating voltage of 20 kV at working distance 10-12 mm. The data obtained for the scans were of high quality and indexing success was high (>90%). Post processing was applied to clean up the data (grain dilation). The misorientation angles were determined according to 2°–5° (subgrain angle boundaries), 5°–15° (low-angle boundaries) and 15°–62.8° (HAGBs).

3. RESULTS

3.1. *Mechanical Behavior (Tensile Testing, Anisotropy)*

The samples in as received condition (H19) and after the annealing processes were subjected to tensile testing at three directions (0º, 45º and 90º) in order to measure the r values. Results are shown in Table

2. According to the results demonstrated in Table 2, the lower Δr value (-0.20) was observed after annealing at H24 condition.

Regarding rm the highest value observed for sheet samples was observed at samples after annealing at H24 and H28 conditions (1.44).

3.2. Microstructural Analysis

The samples were examined in as polished condition in order to examine the amount of second phase particles present, after Barker's etching in order to observe the grains and after HF etching in order to observe the dispersoids and acquire a quantitative conclusion regarding dispersoids. In Figs. 8-16, the evolution of the deformed grains created after the rolling pass is observed. The annealing processes had no effect on the size and distribution of second phase particles [Fig 1. (a)].

The microstructure of the sheet in H19 metallurgic condition was strongly deformed (fibrous) [Fig. 1 (b)], and it was retained in H24 condition.[Fig. 1 (c)]. At a higher recrystallization temperature the microstructure is at the higher fraction recrystallized [Fig. 1 (d)], while at even higher temperature a fully recrystallized microstructure (O sample) is obtained [Fig.1 (e)].

Electrical conductivity (EC) and hardness measurements are shown in Table 2. It is readily observed that conductivity is inversely proportional to hardness (conductivity increases with amount of recrystallization and hardness values are decreasing), since electrical resistance is higher at the presence of dislocations in the cold worked microstructure. It is noteworthy that the very high drops in hardness values are observed from cold worked to H24 metallurgical condition (from 104 to 83 HV0.2 and from the last to the almost completely H28 (from 83 to 54 HV0.2). On the other hand, EC measurements are not so sensitive in showing high differences with the change of the metallurgical state. The EC increased per 1% by the transition from recovered state to the recrystallized. The H19 and H24 sheet samples (≈38 IACS%) exhibited almost the same EC values as well as the H28 and O samples (≈40 IACS%).

The inverse pole figure maps, misorientation angle grain boundaries maps and the grain orientation spread maps are shown in Fig. 2. During annealing process new, strain free grains are formed, while sub- and low grain boundaries are gradually replaced by high angle boundaries. Similarly to hardness, a high decrease in the amount of subgrain boundaries occurs from H19 to H24 metallurgical condition (from 45 to 26%). Interestingly, in the case of sub-grain boundaries the decrease in their amount continues almost with the same rate from H24 to H28 and from H28 to O metallurgical conditions (13 and 11% decrease respectively). In addition the volume fraction of the material with GOS value lower than 1, as indicative measurement of the fully recrystallized grains, is increasing accordingly with the higher value of 83% in the O temper. Thus, it could be considered that for annealed Al sheets GOS values higher than 80% are typical of recrystallization completion (Table 2).

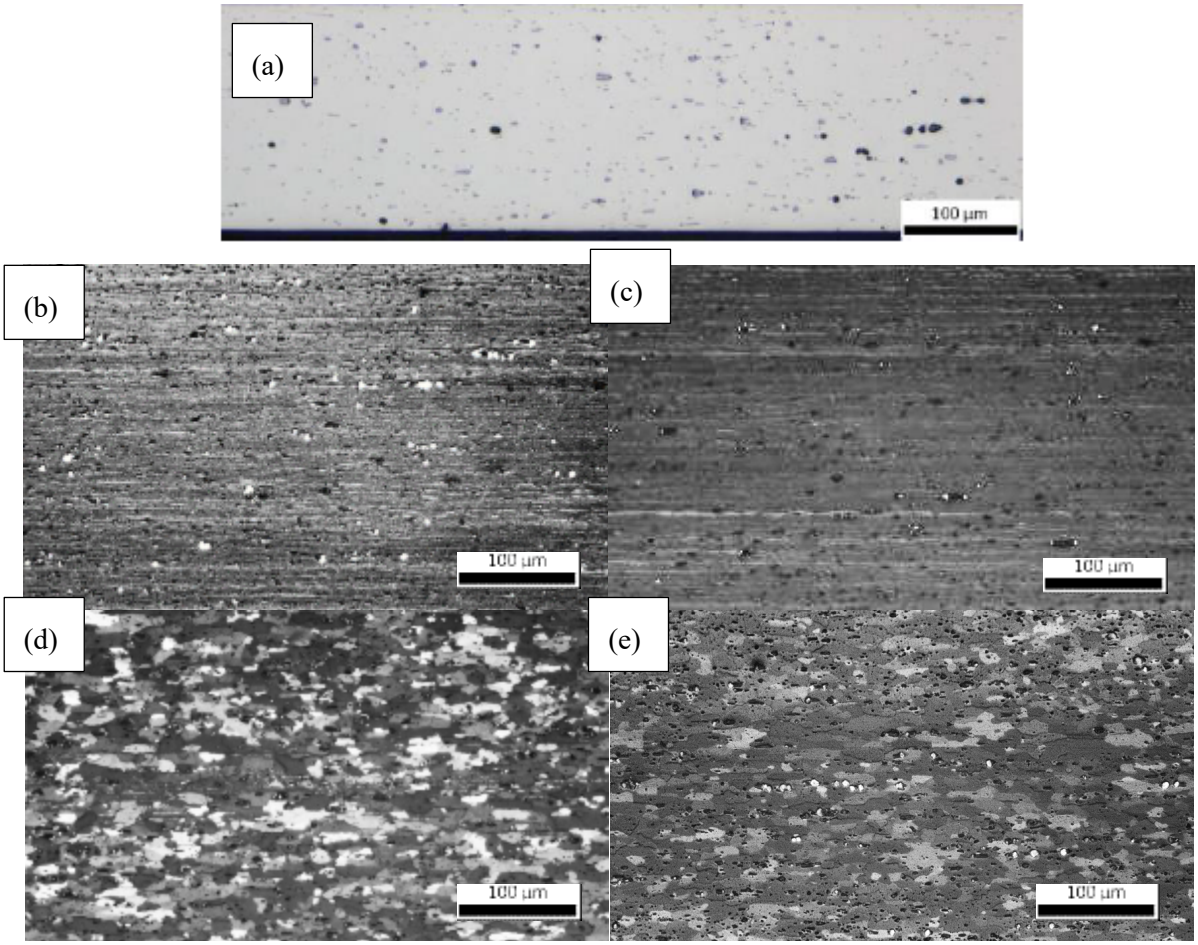


Figure 1. Optical micrographs of the examined samples before and after Barkers electrolytic etching in order to revile the grain structure (a), (b) sample H19, (b) H24, (c) H28 and (d) O.

3.3. EBSD Scans and Analysis

In Tables 3-6 analytical data of the crystallographic texture components of the sheet samples after the thermal treatments are shown. S and Brass constitute the prevailing components in the cold rolled state (>50 vol. %) with Taylor, Dillamore and Copper having 4-11 vol. %) and (101) directions prevail in the respective IPF map. At H24 the highest decrease in % is shown by Taylor component, while only at H28 do S and Brass components start to significantly decrease reaching a total mount of 22 % vol. Interestingly Dillamore exhibited a higher volume fraction in this state compared with H19 and H24, but more measurements should be done for verification of this behaviour.

The total percentage of recrystallization components after each thermal treatment, increased slightly at the lower annealing temperature (6% increase from H19 to H24) and more rapidly at higher temperature (27% increase from H24 to H28). After annealing, the most prominent recrystallization texture components were R (10% vol. in O temper), Goss (11% vol.) and Q (12% vol.).

After each annealing the percentage of sub grain boundaries decreased.

Electrical conductivity (EC) and hardness measurements are shown in Table 2.

Table 2. R-values retrieved from tensile testing at three directions towards rolling direction (parallel, 45° and transverse- three dog bone samples at each direction).

Condition*	*1Δr $=\frac{r_0 + r_{90} - 2r_{45}}{2}$	*2rm=$\frac{r_0 + r_{90} + 2r_{45}}{4}$ *	Conductivity (IACS%)	Hardness $HV_{0.2}$	Rolling texture (%)	Recrystallization texture (%)	Subgrain boundaries (2°-5°) (%)	GOS (%)	
H19	0.05	0.88	38.3	107	74.1	5.6	45.3	**0°-1°**	3.7
								1°-10°	95.1
H24	-0.20	1.44	38.9	83	61.3	11.7	26.4	**0°-1°**	18.7
								1°-10°	66.5
H28	0.03	1.44	39.7	54	41.0	38.2	13.6	**0°-1°**	53.6
								1°-10°	43.3
O	-0.14	1.05	39.8	51	10.7	40.2	2.3	**0°-1°**	83.3
								1°-10°	16.1

***:** According to BS EN 541:2006.

***1**: Planar anisotropy parameter/This is an indicator of the ability of a material to demonstrate a non-earing behavior (lower is better).

*2: This is an excellent indicator of the ability of a material to be deep drawn (higher is better).

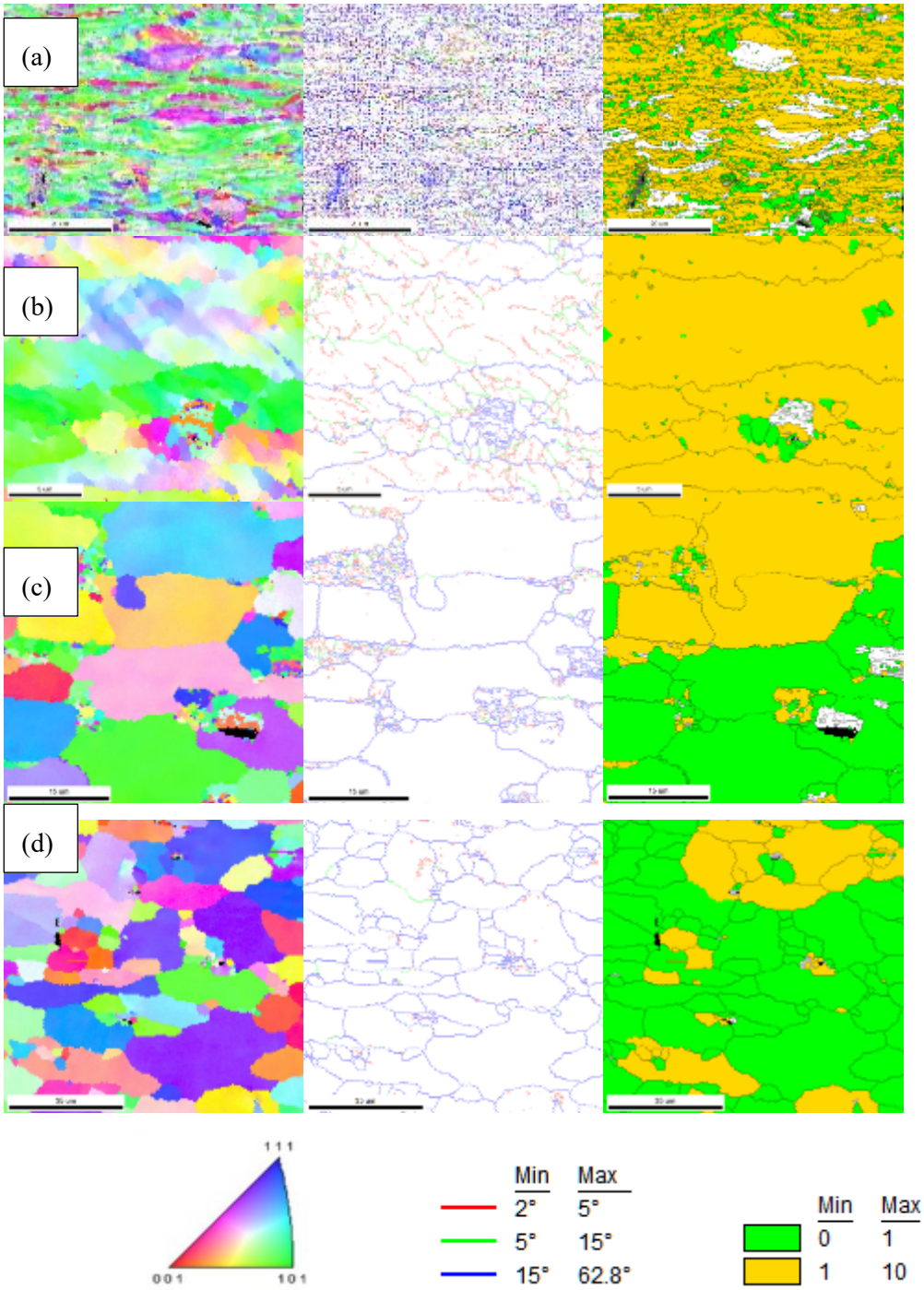


Figure 2. Inverse Pole Figure (IPF) maps, misorientation angle maps and grain orientation spread (GOS) maps of (a) H19, (b) H24, (c) H28 and (O) samples.

Table 3. H19 sample volume fraction of texture components.

Texture	Total	Components %				
Recrystallization	5.6	**Cube (001)[100]**	**P (011)[1-22]**	**Q (013)[2-31]**	**Goss (011)[100]**	**R (214)[-1-21]**
		1.7	1.0	1.4	1.5	
Rolling	74.1	**Copper (112)[111]**	**Taylor**	**S (213)[-11-2315]**	**Dillamore (4411)[-11-118]**	**Brass (011)[211]**
		4.3	10.5	30.9	6.6	**21.8**
Random	20.3					

Table 4. H24 sample volume fraction of texture components.

Texture	Total	Components %				
Recrystallization	11.7	Cube (001)[100]	P (011)[1-22]	Q (013)[2-31]	Goss (011)[100]	R (214)[-1-21]
		0.1	0.1	0.9	3.0	7.6
Rolling	61.3	Copper (112)[111]	Taylor	S (213)[-11-2315]	Dillamore (4411)[-11-118]	Brass (011)[211]
		4.7	1.2	35.4	4.6	15.4
Random	27.0					

Table 5. H28 sample volume fraction of texture components.

Texture	Total	Components %				
Recrystallization	38.2	Cube (001)[100]	P (011)[1-22]	Q (013)[2-31]	Goss (011)[100]	R (214)[-1-21]
		0.7	0.5	15.0	14.0	8.0
Rolling	41.0	Copper (112)[111]	Taylor	S (213)[-11-2315]	Dillamore (4411)[-11-118]	Brass (011)[211]
		5.0	0.5	14.0	13.6	7.9
Random	20.8					

Table 6. O sample volume fraction of texture components.

Texture	Total	Components %				
Recrystallization	40.2	Cube (001)[100]	P (011)[1-22]	Q (013)[2-31]	Goss (011)[100]	R (214)[-1-21]
		2.9	4.8	12.0	10.5	10.0
Rolling	10.7	Copper (112)[111]	Taylor	S (213)[-11-2315]	Dillamore (4411)[-11-118]	Brass (011)[211]
		9.1			0.2	1.4
Random	49.1					

4. DISCUSSION

The lower Δr value for the sheet samples (0.03) was observed after annealing for achieving H28 state, while regarding rm the highest value was observed at samples after annealing at H24 and H28 (1.44). In H19 condition there is a low Δr value (0.05), but the rm value is also considered low (0.88) and therefore the material is not suitable for forming.

The maximum amount of subgrain boundaries that can be calculated in the Al sheets is in H19 condition and they constitute 45% of the total boundaries. In this state the grains which exhibit very low mean misorientation values from the average orientation (lower than 1°) occupy approximately 4% vol. These properties, which are calculated by EBSD are shown to clearly depict the microstructure properties in cold rolled, partially recrystallized and recrystallized conditions and they can be used for observation of recovery and annealing processes.

It is assumed that the highest formability will be exhibited in H28 metallurgical condition where the recrystallization is almost completed and there is a low amount of recovered microstructure. In this state there is a significant balance between rolling and recrystallization texture components volume fractions in the material (38.2 vol. % recrystallization and 41.0 % rolling texture) which is considered as the most preferable condition for earing properties.

The fact that there is a small volume in the material which remains recovered is shown by the presence of 14 % subgrain boundaries and the GOS measurements (54 vol. % with value 0-1°). These properties are highly sensitive to recrystallization process, since in O temper they are significantly altered. On the other hand mechanical properties indices Δr and rm, EC and hardness do not exhibit appreciable differences from H28 state to O temper.

Regarding the microstructural evolution, samples started with strongly deformed microstructure (fibrous), which retained its state after annealing at H24 while the grains were recovered. After annealing at H28, a recrystallized microstructure with small equiaxed grains was observed while, a zone of approximately 50 μm retained the previous deformed microstructure. The final thermal treatment, lead to a fully recrystallized microstructure, with coarse equiaxed grains through thickness.

Regarding the second phase particles, no significant difference was observed among the samples examined before and after the annealing processes. The increase of EC of sample was evident after annealing at H28 and could be attributed to fewer substructural obstacles such as dislocation tangles.

5. CONCLUSIONS

From the above findings the following conclusions could be derived:

- The highest formability of the AA3104 sheet is expected at H28 metallurgical condition. In this state the sheet is almost completely recrystallized, but a limited volume fraction remains in recovered state. Consequently even if the volume percentage of recrystallization texture components has been already formed, an equivalent volume of rolling texture is present and this balance leads to the highest formability properties, as indicated by the lowest Δr and highest rm values in tensile testing.
- EBSD analysis proved a powerful technique in presenting and calculation of recrystallization volumes from cold rolled to fully recrystallized states, while the most proper measurements, which were sensitive to metallurgical state alterations, were % of subgrain boundaries and GOS.
- In the deformed state the grain structure was fibrous, and it was in H24 as viewed by optical microscopy, however with EBSD the differences in the microstructure are readily observed and also measurable.
- The presence of subgrain boundaries is related not only with a recovered state, but mostly with the hard temper.

- Hardness and EC constitute properties that allow the viewing of the metallurgical condition change from H19 to H28, but from H28 to O temper they cannot be used for safe conclusions.

ACKNOWLEDGMENTS

The authors would like to express their gratitude to ELKEME S.A. and ELVAL S.A. managements for all the kind support.

REFERENCES

1. Huffman, LM 1996, "Processing whey protein for use as a food ingredient", *Food Technology*, vol. 50, no. 2, pp. 49-52.
2. S. Papadopoulou, A. Kontopoulou, E. Gavalas, and S. Papaefthymiou. 2020. "The Effects of Reduction and Thermal Treatment on the Recrystallization and Crystallographic Texture Evolution of 5182 Aluminum Alloy" Metals 10, no. 10: 1380. https://doi.org/10.3390/met10101380.
3. University of Queensland Library 2009, *Mechanical engineering subject guide*, University of Queensland Library, viewed 6 February 2009, <http://www.library.uq.edu.au/findits/findit.php?title=Mechanical+Engineering>.
4. U. F. Kocks, C. N. Tome and H. R. Wenk, Texture and Anisotropy, CAMBRIDGE UNIVERSITY PRESS, 2000.
5. D. F. I.Tikhovskiy, "Simulation of earing during deep drawing of an Al–3% Mg alloy (AA 5754) using a texture component crystal plasticity FEM," Journal of Materials Processing Technology, vol. 183, no. 2-3, 23 March 2007.
6. F. Humphreys and M. Hatherly, Recrystallization and related annealing phenomena, Elsevier, 2004.
7. M. Peters, K. Welpmann and T. Sanders Jr, Advanced Materials Research and Developments for Transport Light Metals, vol. 20, Les Ulis: Les Editions, 1985, pp. 259-264.
8. Z. Zhao, "A texture optimization study for minimum earing in aluminium by use of a texture component crystal plasticity finite element method," Acta Materialia, vol. 52, 2004.
9. OIM Analysis 5.3 Manual.
10. S. Papadopoulou, E. Gavalas, and S. Papaefthymiou. 2021. "Methodology for the Identification of Nucleation Sites in Aluminum Alloy by Use of Misorientatation Mapping" Materials Proceedings 3, no. 1: 11. https://doi.org/10.3390/IEC2M-09251.
11. S. Papadopoulou, V. Loukadakis, Z. Zacharopoulos, and S. Papaefthymiou. 2021. "Influence of Uniaxial Deformation on Texture Evolution and Anisotropy of 3104 Al Sheet with Different Initial Microstructure" Metals 11, no. 11: 1729. https://doi.org/10.3390/met11111729.
12. O. Daaland and E. Nes, "Origin of Cube texture during hot rolling of commercial Al-Mn-Mg alloys," Acta Materialia, vol. 44, no. 4, pp. 1389-1411, 1995.
13. Y. Li and L. Arnberg, "Quantitative study on the precipitation behavior ofdispersoids in DC-cast AA3003 alloy during heating and homogenization," Acta Materialia, vol. 51, pp. 3415-3428, 2003.
14. P. Rossiter, The Electrical Resistivity of Metals and Alloys, Cambridge: Cambridge University Press, 1987.
15. Y. Li and L. Arnberg, "Quantitative study on the precipitation behavior of dispersoids in DC-cast AA3003 alloy during heating and homogenization," Acta Materialia, vol. 51, pp. 3415-3428, 2003.
16. S. Vooijs, S. Davenport, I. Todd and S. Van der Zwaag, "Monitoring the precipitation reactions in a cold-rolled Al–Mn–Mg–Cu alloy using thermoelectric power and electrical resistivity measurements," Philosophical Magazine A, vol. 81, no. 8, pp. 2059-2072, 2001.

17. D. Askeland, The science and engineering of materials, Seventh ed., Vols. 286-288, Boston, MA: The Wright, Wendelin J. (Seventh ed.), 2015.
18. Y. Li, A. Muggerud, A. Olsen and T. Furu, "Precipitation of partially coherent α-Al(Mn,Fe)Si dispersoids and their strengthening effect in AA 3003 alloy," Acta Materialia, vol. 60, no. 3, pp. 1004-1014, 2012.
19. Y. Li and L. Arnber, "Precipitation of Dispersoids in DC-Cast 3003 Alloy," Materials Science Forum, Vols. 396-402, pp. 875-880, 2002.
20. Y. Li and L. Arnberg, "Precipitation of Dispersoids in DC-Cast AA3103 Alloy during Heat Treatment BT," Essential Readings in Light Metals, vol. 3, pp. 1021-1027, 2016.
21. G. F. V. VOORT, Metallography, Principles and Practice, New York: McGraw-Hill, 1984.
22. ASTM E407 - 07 (2015) Standard Practice for Microetching Metals and Alloys, ASTM International.
23. "British standard Aluminium and aluminium alloys —Rolled products for cans, closures and lids — Specifications "BS EN 541:2006, [Online]. Available: http://106.38.59.21:8080/userfiles/ba7f31b84bf14fc8b9ace13a7e23a2e1/files/teckSolution/2021/05/EN%20541-2006.pdf.
24. https://www.matweb.com/search/datasheet_print.aspx?matguid=aaaabe41a20a4ed2b48270f7f2ef1b2d
25. "Standard Test Method for Tensile Strain – Hardening Exponents (n – Values) of Metallic Sheet Materials, ASTM, United States ", Astm.org, 2021. [Online]. Available: https://www.astm.org/Standards/E646.htm.
26. "Standard Test Method for Plastic Strain Ratio r for Sheet Metal, ASTM, Designation E 517-00, United States", Astm.org, 2021. [Online]. Available: https://www.astm.org/Standards/E517.htm.
27. J. Hirsch and O. Engler, "Texture, local orientation and microstructure in industrial Al-alloys," Roskilde, 1995.
28. H. Takeda, A. Hibino and K. Takata, "Influence of Crystal Orientations on the Bendability of an Al-Mg-Si Alloy," Materials Transactions, vol. 51, 2010.
29. G. E. Dieter, Mechanical Metallurgy, McGraw-Hill Book Company, 1988.
30. K. Liu and X. Chen, "Influence of heat treatment and its sequence on elevatedtemperature properties of Al-Mn-Mg 3004 alloy," Materials Science and Engineering: A, vol. 697, pp. 141-148, 2017.
31. Y. Li, A. Muggerud, A. Olsen and T. Furu, "Precipitation of partially coherent αAl(Mn,Fe)Si dispersoids and their strengthening effect in AA 3003 alloy," Acta Materialia, vol. 60, pp. 1004-1014, 2012.
32. A. Muggerud, E. Mørtsell, Y. Li and R. Holmestad, "Dispersoid strengthening in AA3xxx alloys with varying Mn and Si content during annealing at low temperatures," Materials Science and Engineering: A, vol. 567, pp. 21-28, 2013.
33. Y. Li and L. Arnberg, "Quantitative study on the precipitation behavior of dispersoids in DC-cast AA3003 alloy during heating and homogenization," Acta Materialia, vol. 51, pp. 3415-3428, 2003.
34. L. Lodgaard and N. Ryum, "Precipitation of dispersoids containing Mn and/or Cr in Al–Si alloys," Material Science and Engineering: A, vol. 283, pp. 144-152, 2000.
35. Y. Li and L. Arnberg, "Solidification structure of DC-cast AA3003 alloy and its influence on homogenization," aluminium, vol. 78, no. 834, 2002.